Journal of Alloys and Compounds 527 (2012) 25–29

Contents lists available at SciVerse ScienceDirect

Journal of Alloys and Compounds

journal homepage: www.elsevier.com/locate/jallcom

Upconversion white luminescence of TeO_2:Tm^{3+}/Er^{3+}/Yb^{3+} nanoparticles

Hui Hu, Yan Bai*

Department of Chemistry, Jinan University, Guangzhou 510632, People's Republic of China

ARTICLE INFO

Article history:
Received 10 July 2011
Received in revised form 17 February 2012
Accepted 24 February 2012
Available online xxx

Keywords:
Upconversion
White luminescence
Rare earth
TeO_2 nanoparticles

ABSTRACT

In this study, TeO_2:Tm^{3+}/Er^{3+}/Yb^{3+} nanoparticles had been successfully prepared via a hydrothermal process. All the as-prepared TeO_2:Tm^{3+}/Er^{3+}/Yb^{3+} nanoparticles showed the blue (476 nm), green (525 nm, 545 nm) and red (667 nm) emissions under 980 nm excitation, which were attributed to the $^1G_4 \rightarrow {}^3H_6$ (Tm^{3+}), $^2H_{11/2}$, $^4S_{3/2} \rightarrow {}^4I_{15/2}$ (Er^{3+}) and $^4F_{9/2} \rightarrow {}^4I_{15/2}$ (Er^{3+}) transitions, respectively. The decay lifetime of blue, green and red emissions were 40 μs, 46 μs and 89 μs, respectively. The combination of blue, green and red emissions resulted in the white luminescence which was intense and visible to the naked eyes. The calculated CIE color coordinates of TeO_2:Tm^{3+}/Er^{3+}/Yb^{3+} nanoparticles fell well within the white region and changed little with the incident pump power from 1.75 W/cm^2 to 16.13 W/cm^2, which indicated that the materials may have potential applications in the fields of three dimensional displays, back lighting, white light sources, and so on.

1. Introduction

Sources of white light has been wide studied since it find applications in many fields, such as three dimensional displays, long lifetime, low-energy light sources, back light and so on [1–11]. One of the effective ways of generating white light is the upconversion in which near-infrared excitation is converted into a visible emission through lanthanide doping. The excitation source of upconversion is an infrared laser, which is compact, power-rich, inexpensive, and can be commercially available. Up to now, there have been several reports on upconversion white luminescence from Tm^{3+}/Er^{3+}/Yb^{3+} or Tm^{3+}/Ho^{3+}/Yb^{3+} doped glasses/powders/ceramic/nanocrystals, such as tellurite glasses [9,10], Y_2O_3 nanocrystals [11], Y_2O_3 transparent ceramic [12], Lu_2O_3 nanocrystals [13], $GdVO_4$ nanocrystals [14], KY_3F_{10} nanocrystals [4], $CaSnO_3$ powders [15], $Gd_4O_3F_6$ nanocrystals [16], $NaYF_4$ nanorods [17] and fluoride glasses [18,19]. For example, Zhang's group studied color control and white light generation of upconversion luminescence by operating dopant concentrations and pump densities in Tm^{3+}/Er^{3+}/Yb^{3+} tri-doped Lu_2O_3 nanocrystals [13]. Li et al. presented upconversion white color output from both the Tm^{3+}/Er^{3+}/Yb^{3+} and Tm^{3+}/Ho^{3+}/Yb^{3+} triply doped $NaYF_4$ nanorods [17]. However, the host materials that are suitable for upconversion white luminescence are still limited and need to be further explored. Selecting a suitable host is a key factor for upconversion luminescent materials. It is well known that TeO_2 (optical fibers, crystals and glassy) are suitable host materials due to their lower phonon frequency, chemical durability and thermal stability [20–29]. The conventional processing is using bulk TeO_2 or TeO_2 glasses as the host materials for preparing upconversion luminescent materials [9,30,31]. For example, Desirena et al. have reported white light upconversion emission in Tm^{3+}/Ho^{3+}/Yb^{3+} co-doped TeO_2 glasses [9]. Bilir et al. have reported the optical properties and upconversion luminescence of Er^{3+} ions in TeO_2–CdF_2–WO_3 glasses [31]. Nanoscale upconversion luminescent materials prepared using nanoparticles as the host materials have attracted much interest because their optical properties, such as lifetime improvement and spectral stability, are different from those of the bulk samples. In our latest research, we reported the preparation of TeO_2 (α-TeO_2, β-TeO_2) nanoparticles in a mild condition [32]. Furthermore, TeO_2:Er^{3+}/Yb^{3+} upconversion luminescent nanoparticles were successfully prepared [33].

In this study, TeO_2 nanoparticles were used as the host materials to prepare Tm^{3+}, Er^{3+} and Yb^{3+} ions co-doped upconversion luminescent materials. The TeO_2:Tm^{3+}/Er^{3+}/Yb^{3+} nanoparticles could give white luminescence. The blue emission was obtained from the Tm^{3+} ions, while the green and red emissions came from the Er^{3+} ions with the Yb^{3+} ions as sensitizers.

2. Experimental

2.1. Materials

Chemicals were all analytical grade. Ytterbium oxide (Yb_2O_3), thulium oxide (Tm_2O_3) and erbium oxide (Er_2O_3) with purity of 99.99% were purchased from Minmetals (Beijing) Rare Earth Institute Company. Sodium tellurite (Na_2TeO_3), gallic acid (GA), acetum (HAc) and nitric acid (HNO_3) were purchased from Aladdin Chemical Corporation. Double-distilled water was used to prepare the solutions. All the materials were used without further purification.

* Corresponding author. Tel.: +86 2088561095.
E-mail address: tbaiyan@jnu.edu.cn (Y. Bai).

0925-8388/$ – see front matter © 2012 Elsevier B.V. All rights reserved.
doi:10.1016/j.jallcom.2012.02.129

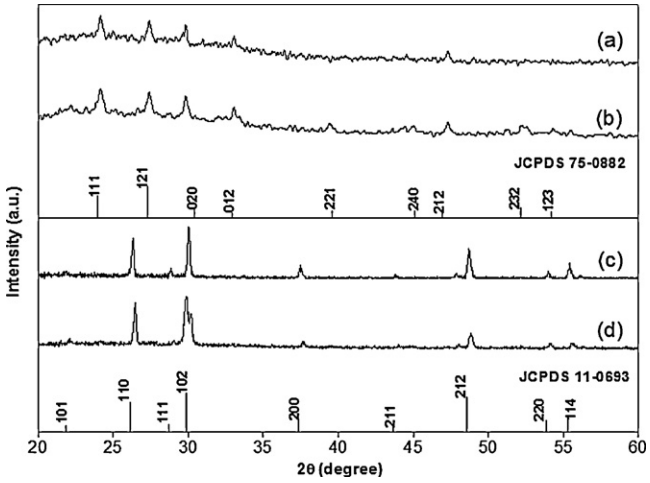

Fig. 1. XRD patterns of (a) β-TeO_2:Tm^{3+}/Er^{3+}/Yb^{3+} (0.5/0.25/10 mol%) nanoparticles, (b) β-TeO_2 nanoparticles, (c) α-TeO_2:Tm^{3+}/Er^{3+}/Yb^{3+} (0.5/0.25/10 mol%) nanoparticles, and (d) α-TeO_2 nanoparticles.

2.2. Preparation of TeO_2:Tm^{3+}/Er^{3+}/Yb^{3+} nanoparticles

The appropriate amounts of Tm_2O_3, Er_2O_3 and Yb_2O_3 powders were dissolved in dilute HNO_3 solution to prepare 0.02 M $Tm(NO_3)_3$, 0.02 M $Er(NO_3)_3$ and 0.02 M $Yb(NO_3)_3$ solutions, respectively. Then, a volume of 10 mL solution of 0.1 M Na_2TeO_3 was added into 20 mL solution of 0.1 M HAc to prepare α-TeO_2 nanoparticles sol. A volume of 10 mL solution of 0.1 M Na_2TeO_3 was added into 20 mL solution of 0.1 M GA to prepare β-TeO_2 nanoparticles sol [32]. In a typical procedure for the preparation of upconversion luminescent α-TeO_2:Tm^{3+}/Er^{3+}/Yb^{3+} (0.5/0.25/10 mol%) nanoparticles, the appropriate amounts of 0.02 M $Tm(NO_3)_3$, 0.02 M $Er(NO_3)_3$ and 0.02 M $Yb(NO_3)_3$ were added into the α-TeO_2 nanoparticles sol. After stirring for 20 min, the as-obtained mixing solution was transferred into a reaction kettle and hydrothermal reacted at 180 °C for 18 h. As the reaction kettles cooled to room temperature naturally, the precipitate was separated by centrifugation, washed with deionized water, dried under vacuum for 24 h and sintered at 600 °C for 2 h to obtain α-TeO_2:Tm^{3+}/Er^{3+}/Yb^{3+} (0.5/0.25/10 mol%) nanoparticles. A similar procedure was used for the preparation of β-TeO_2:Tm^{3+}/Er^{3+}/Yb^{3+} (0.5/0.25/10 mol%) nanoparticles.

2.3. Characterization

Transmission electron microscopy (TEM; TECNAL-10, PHILIPS) technique and Zetasizer (Nano-ZS; Malvern Instruments Ltd.) were used to observe the morphology and size of the as-prepared samples. The applied voltage and magnification of transmission electron microscopy technique were 100 kV and 100,000 times, respectively. X-ray diffraction (XRD) measurement was used to characterize the crystallization of the as-prepared samples. The source of radiation was Kα radiancy of copper at 36 kV and 20 mA in the range of 10–80° by step scanning with a step size of 0.02° (MSAL XD-2, Beijing University, China). Upconversion luminescence spectra were used to investigate the optical property of the as-prepared samples. Upconversion luminescence spectra were obtained using a 980 nm laser from a fiber coupled laser (VA-I-N, Beijing Top Technology Company, China) and detected by fluorescence spectrophotometer (F-4500, Hitachi, China). Luminescence decay curves were obtained from a spectrofluorimeter (Triax 320, Jobin-Yvon, France).

3. Results and discussion

3.1. Phase and morphology

Fig. 1 showed the X-ray diffraction (XRD) patterns of TeO_2:Tm^{3+}/Er^{3+}/Yb^{3+} nanoparticles. All the peaks of α-TeO_2:Tm^{3+}/Er^{3+}/Yb^{3+} nanoparticles (Fig. 1c) and β-TeO_2:Tm^{3+}/Er^{3+}/Yb^{3+} nanoparticles (Fig. 1a) could be indexed as the tetragonal phase α-TeO_2 (Fig. 1d) and the orthorhombic phase β-TeO_2 (Fig. 1b) according to the Joint Committee on Powder Diffraction Standards (JCPDS) file 11-0693 and 75-0882, respectively. The results indicated that the TeO_2 nanoparticles kept the original phase after having been co-doped Tm^{3+}/Er^{3+}/Yb^{3+} ions.

As shown in Fig. 2, α-TeO_2:Tm^{3+}/Er^{3+}/Yb^{3+} (0.5/0.25/10 mol%) nanoparticles were irregular flakes with the particle diameter ranging from 40 to 400 nm (Fig. 2a) and β-TeO_2:Tm^{3+}/Er^{3+}/Yb^{3+} (0.5/0.25/10 mol%) nanoparticles were ellipsoidal with the particle diameter ranging from 30 to 200 nm (Fig. 2b). The particles size distribution was further determined by Zetasizer using dynamic light scattering (Fig. 3). The average diameters of α-TeO_2:Tm^{3+}/Er^{3+}/Yb^{3+} nanoparticles and β-TeO_2:Tm^{3+}/Er^{3+}/Yb^{3+}

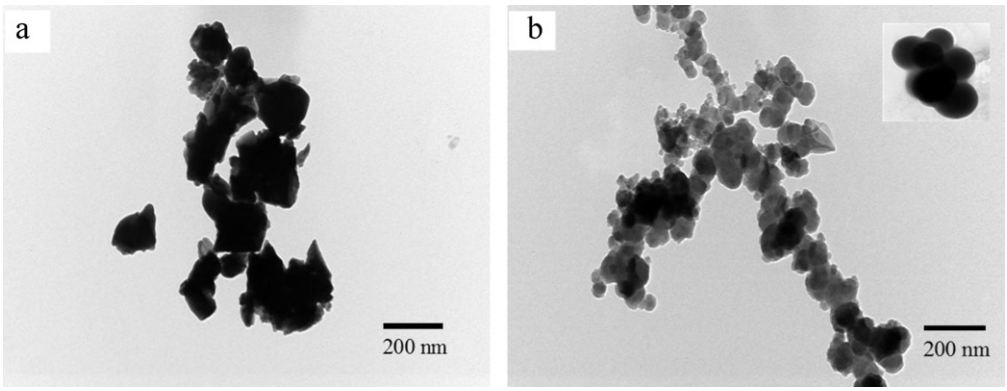

Fig. 2. TEM images of (a) α-TeO_2:Tm^{3+}/Er^{3+}/Yb^{3+} (0.5/0.25/10 mol%) nanoparticles and (b) β-TeO_2:Tm^{3+}/Er^{3+}/Yb^{3+} (0.5/0.25/10 mol%) nanoparticles.

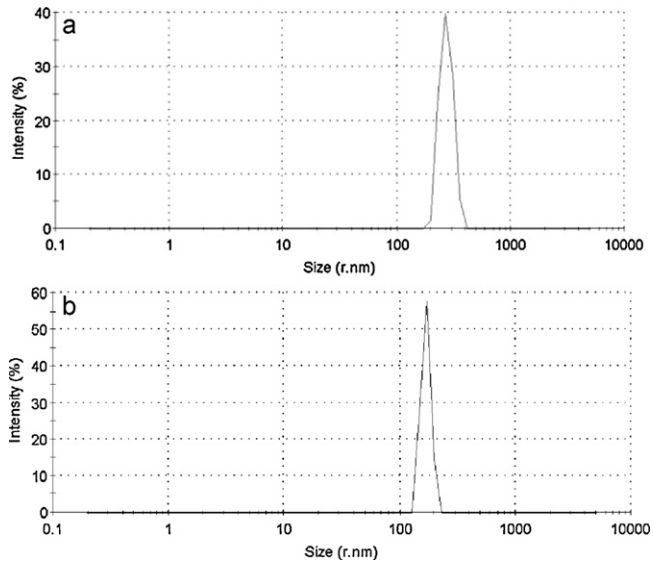

Fig. 3. Particle size analysis of (a) α-TeO_2:Tm^{3+}/Er^{3+}/Yb^{3+} (0.5/0.25/10 mol%) nanoparticles and (b) β-TeO_2:Tm^{3+}/Er^{3+}/Yb^{3+} (0.5/0.25/10 mol%) nanoparticles.

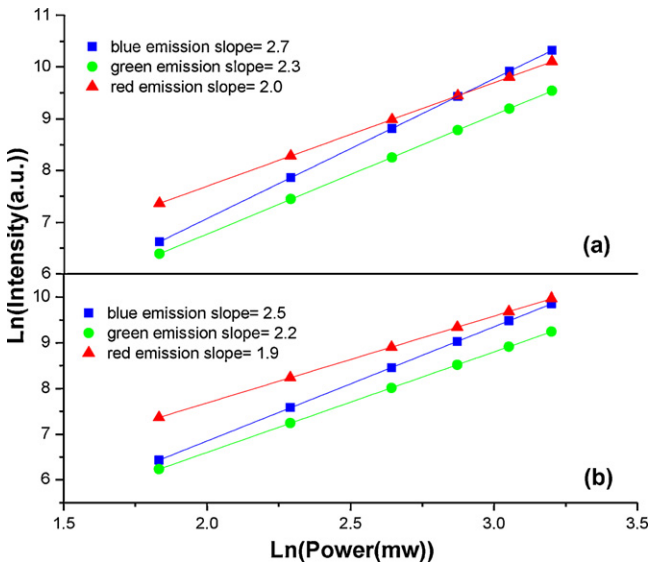

Fig. 5. Power dependence of upconversion emission intensities of (a) α-TeO_2:Tm^{3+}/Er^{3+}/Yb^{3+} (0.5/0.25/10 mol%) nanoparticles and (b) β-TeO_2:Tm^{3+}/Er^{3+}/Yb^{3+} (0.5/0.25/10 mol%) nanoparticles.

nanoparticles were found to be 272.6 nm and 168.5 nm, respectively. The results indicated that the TeO_2 nanoparticles mainly kept the original morphology after having been co-doped Tm^{3+}/Er^{3+}/Yb^{3+} ions.

3.2. Upconversion emission properties

Fig. 4 showed the upconversion emission spectra in the range 400–800 nm under 980 nm excitation. The sharp blue emission around 476 nm was attributed to the $^1G_4 \rightarrow {}^3H_6$ transition of Tm^{3+} ions. The green emissions around 525 nm and 545 nm were attributed to the $^2H_{11/2} \rightarrow {}^4I_{15/2}$ and $^4S_{3/2} \rightarrow {}^4I_{15/2}$ transitions of the Er^{3+} ions, respectively. The red emission around 667 nm was attributed to the $^4F_{9/2} \rightarrow {}^4I_{15/2}$ transition of Er^{3+} ions and the $^3F_2 \rightarrow {}^3H_6$ transition of Tm^{3+} ions.

In order to understand the upconversion mechanisms of the observed emission bands, the upconversion emission intensity was measured as a function of excitation intensity. Fig. 5 showed the dependence of the upconversion emission intensities (I_{up}) on excitation intensity (P) of the as-prepared samples. The calculated results indicated that slopes value of α-TeO_2:Tm^{3+}/Er^{3+}/Yb^{3+} (0.5/0.25/10 mol%) nanoparticles were 2.7 and 2.0 for blue ($^1G_4 \rightarrow {}^3H_6$), and red ($^4F_{9/2} \rightarrow {}^4I_{15/2}$) emissions, respectively, which showed that the upconversion mechanism corresponding to blue and red emissions occurred via a three-photon and a two-photon, respectively. There were two possible processes (two-photon or three-photon process) for the green emission [34]. The slope value of the green emission ($^2H_{11/2} \rightarrow {}^4I_{15/2}$) was 2.3, which indicated the upconversion mechanism corresponding to green emission occurred mainly via a two-photon. The slopes value of β-TeO_2:Tm^{3+}/Er^{3+}/Yb^{3+} (0.5/0.25/10 mol%) nanoparticles were 2.5 and 1.9 for blue ($^1G_4 \rightarrow {}^3H_6$), and red ($^4F_{9/2} \rightarrow {}^4I_{15/2}$) emissions, respectively, which showed that the upconversion mechanism corresponding to blue and red emissions occurred via a three-photon and a two-photon, respectively. The slope value of the green emission ($^2H_{11/2} \rightarrow {}^4I_{15/2}$) was 2.2, which indicated the upconversion mechanism corresponding to green emission occurred mainly via a two-photon in the same as those of α-TeO_2:Tm^{3+}/Er^{3+}/Yb^{3+} (0.5/0.25/10 mol%) nanoparticles.

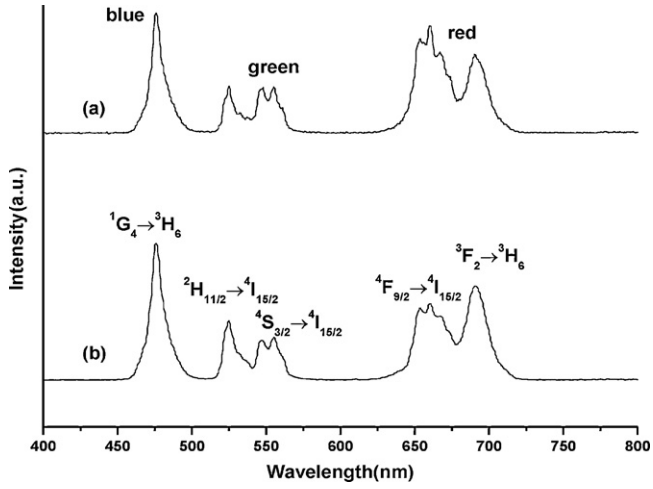

Fig. 4. Upconversion emission spectra of (a) α-TeO_2:Tm^{3+}/Er^{3+}/Yb^{3+} (0.5/0.25/10 mol%) nanoparticles and (b) β-TeO_2:Tm^{3+}/Er^{3+}/Yb^{3+} (0.5/0.25/10 mol%) nanoparticles under 980 nm excitation.

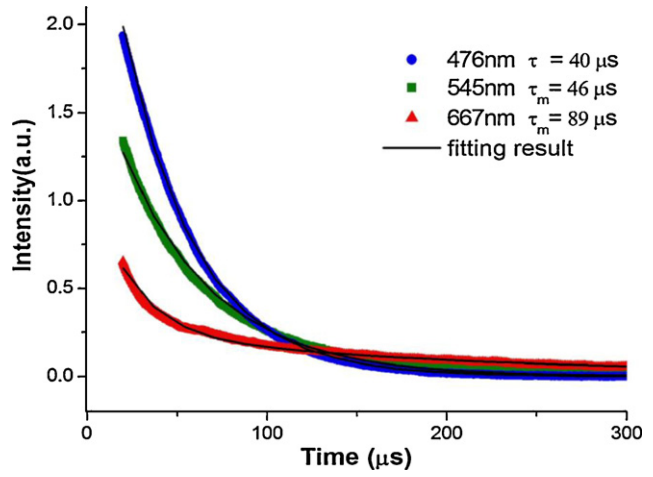

Fig. 6. Luminescence decay curves of blue (Tm^{3+}: $^1G_4 \rightarrow {}^3H_6$), green ($Er^{3+}$: $^4S_{3/2} \rightarrow {}^4I_{15/2}$) and red ($Er^{3+}$: $^4F_{9/2} \rightarrow {}^4I_{15/2}$) emissions of α-$TeO_2$:$Tm^{3+}$/$Er^{3+}$/$Yb^{3+}$ (0.5/0.25/10 mol%) nanoparticles under 980 nm excitation.

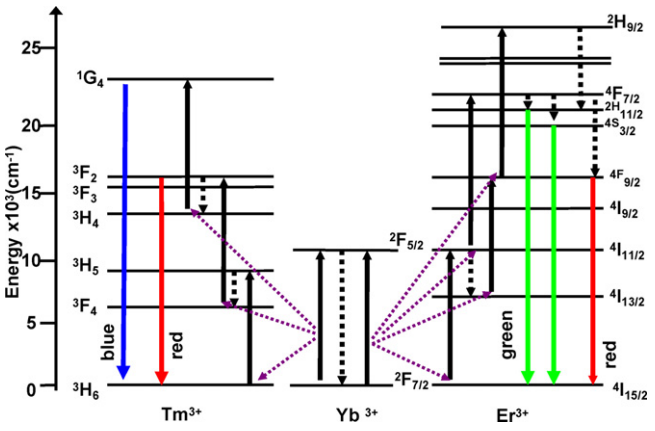

Fig. 7. Energy level diagrams of Tm^{3+}, Er^{3+}, and Yb^{3+} ions and the proposed UC emission mechanism.

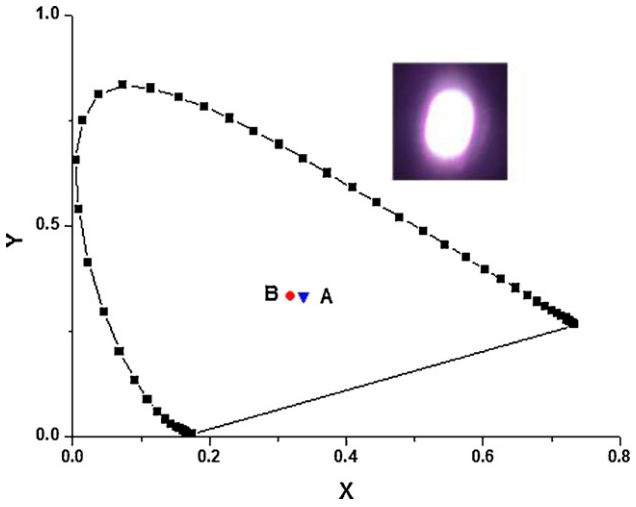

Fig. 8. CIE chromaticity diagrams of 1931 together with the calculated color coordinates for (A) α-TeO_2:Tm^{3+}/Er^{3+}/Yb^{3+} (0.5/0.25/10 mol%) nanoparticles and (B) β-TeO_2:Tm^{3+}/Er^{3+}/Yb^{3+} (0.5/0.25/10 mol%) nanoparticles.

Fig. 6 showed the blue ($^1G_4 \rightarrow {}^3H_6$), green ($^4S_{3/2} \rightarrow {}^4I_{15/2}$) and red ($^4F_{9/2} \rightarrow {}^4I_{15/2}$) upconversion luminescence decay curves of α-TeO_2:Tm^{3+}/Er^{3+}/Yb^{3+} (0.5/0.25/10 mol%) nanoparticles at 476 nm, 545 nm and 667 nm emissions under 980 nm excitation. The 476 nm blue emission was single exponential fitting with a lifetime of 40 μs (correlation coefficient: $R^2 = 0.9997$), which was shorter than that (196 μs) of the same emission of Lu_2O_3:Tm^{3+}/Er^{3+}/Yb^{3+} (0.2/0.4/3 mol%) nanocrystals [35]. The 545 nm green emission was fitted by a double exponential function, which can be expressed as follows:

$$I(t) = I_0 + A_f\ e^{-t/\tau_f} + A_s\, e^{-t/\tau_s} \quad (1)$$

where $I(t)$ is the luminescence intensity at the time t, τ_f and τ_s are the luminescent lifetimes of the fast and slow stages, A_f and A_s are the weight factors of the two components, respectively. I_0 is the background light intensity [36]. The fitting parameters were $\tau_f = 24$ μs, $\tau_s = 157$ μs, and $A_f/A_s = 10.75$ (correlation coefficient: $R^2 = 0.9983$). The mean decay lifetime (τ_m) is given by,

$$\tau_m = \int_{t0}^{\infty} \frac{I(t)}{I_{\max}} dt \quad (2)$$

where $I_{\max}$ is the maximum of $I(t)$ ($I_{\max} = I(t_0 = 0)$) [37]. The mean decay lifetime (τ_m) was 46 μs, which was longer than that (12.8 μs) of the same emission of Lu_2O_3:Tm^{3+}/Er^{3+}/Yb^{3+} (0.6/0.8/8 mol%) nanocrystals [38]. The 667 nm red emission was also fitted by a double exponential function. The fitting parameters were $\tau_f = 22$ μs, $\tau_s = 197$ μs, and $A_f/A_s = 3.64$ (correlation coefficient: $R^2 = 0.9962$). The mean decay lifetime (τ_m) was 89 μs. The A_f/A_s values from the 545 nm green and 667 nm red emissions indicated that both excited state absorption and energy transfer approaches could contribute to the upconversion emission of Er^{3+} ions [37]. Similar results were also observed for β-TeO_2:Tm^{3+}/Er^{3+}/Yb^{3+} (0.5/0.25/10 mol%) nanoparticles.

The upconversion mechanisms in TeO_2:Tm^{3+}/Er^{3+}/Yb^{3+} nanoparticles had been well investigated. Fig. 7 was the schematic energy level diagram of Tm^{3+}, Er^{3+} and Yb^{3+} ions. As indicated in Fig. 7, the Yb^{3+} ions were excited to the $^2F_{5/2}$ state from the ground state $^2F_{7/2}$, then transferred the energy to Er^{3+} or Tm^{3+} ions, while the Er^{3+} ions also absorbed 980 nm photons. For the red ($^4F_{9/2} \rightarrow {}^4I_{15/2}$) and green ($^2H_{11/2} \rightarrow {}^4I_{15/2}$, $^4S_{3/2} \rightarrow {}^4I_{15/2}$) emissions of Er^{3+} ions, an initial energy from Yb^{3+} ions ($^2F_{5/2}$) excited Er^{3+} ions ($^4I_{15/2}$) to the $^4I_{11/2}$ states. Subsequent nonradiative relaxations of Er^{3+} ($^4I_{11/2}$) → Er^{3+} ($^4I_{13/2}$) occurred. Then, a second 980 nm photon from the excited Yb^{3+} ions excited Er^{3+} ions ($^4I_{13/2}$, $^4I_{11/2}$) to Er^{3+} ions ($^4F_{9/2}$, $^4F_{7/2}$). The Er^{3+} ions in the $^4F_{7/2}$ states relaxed nonradiatively by a fast multiphoton decay process to the $^2H_{11/2}$ and $^4S_{3/2}$ states, then the dominant green ($^2H_{11/2} \rightarrow {}^4I_{15/2}$, $^4S_{3/2} \rightarrow {}^4I_{15/2}$) emissions occurred. Alternatively, the Er^{3+} ions in the $^4F_{9/2}$ states mainly relaxed radiatively to the ground states $^4I_{15/2}$, which caused red emissions. Another mechanism happened involving a three-photon process to green upconversion emission. A third 980 nm photon from Yb^{3+} ions excited Er^{3+} ($^4F_{9/2}$) ions to Er^{3+} ($^2H_{9/2}$) ions. The Er^{3+} ions in the $^2H_{9/2}$ states relaxed nonradiatively by a fast multiphoton decay process to the $^2H_{11/2}$ and $^4S_{3/2}$ states, and the dominant green ($^2H_{11/2} \rightarrow {}^4I_{15/2}$, $^4S_{3/2} \rightarrow {}^4I_{15/2}$) emissions occurred. The blue emission ($^1G_4 \rightarrow {}^3H_6$) of Tm^{3+} ions was attributed to the effective energy transfer from Yb^{3+} ions to Tm^{3+} ions through the three-step energy transfer. Under excitation at 980 nm, firstly, an initial energy transferred from Yb^{3+} ($^2F_{5/2}$) ions to Tm^{3+} ($^3H_6$) ions and the Tm^{3+} ($^3H_6$) ions were excited to the $^3H_5$ states. Subsequent nonradiative relaxations of Tm^{3+} ($^3H_5$) → Tm^{3+} ($^3F_4$) occurred. A second energy transferred from Yb^{3+} ($^2F_{5/2}$) ions excited Tm^{3+} ($^3F_4$) ions to the $^3F_2$ states. Subsequent nonradiative relaxations of Tm^{3+} ($^3F_2$) → Tm^{3+} ($^3H_4$) occurred. Then, a third 980 nm photon from Yb^{3+} ions excited Tm^{3+} ($^3H_4$) ions to Tm^{3+} ($^1G_4$) ions. Then, the strong blue emission ($^1G_4 \rightarrow {}^3H_6$) and weak red emissions ($^3F_2 \rightarrow {}^3H_6$) occurred.

To measure the color of the visible emission, the Commission internationale de l'éclairage (CIE) coordinates were calculated. The CIE was the standard reference for defining colors and was obtained by considering the sensitivity of the human eye to different colors (wavelengths). The calculated color coordinates A (0.34, 0.33) for the α-TeO_2:Tm^{3+}/Er^{3+}/Yb^{3+} (0.5/0.25/10 mol%) nanoparticles and B (0.32, 0.33) for the β-TeO_2:Tm^{3+}/Er^{3+}/Yb^{3+} (0.5/0.25/10 mol%) nanoparticles measured under the pump power of 36.4 W/cm^2 fell well within the white region of the CIE diagram (Fig. 8). The inset in Fig. 8 displayed a digital photograph of the upconversion white luminescence of the α-TeO_2:Tm^{3+}/Er^{3+}/Yb^{3+} (0.5/0.25/10 mol%) nanoparticles. The sample showed a strong white luminescence demonstrating the high efficiency of the upconversion process. Fig. 9 showed the upconversion emission spectra and the 1931 CIE chromaticity diagram together with the calculated color coordinates of α-TeO_2:Tm^{3+}/Er^{3+}/Yb^{3+} (0.5/0.25/10 mol%) nanoparticles measured under different pump power. The calculated color coordinates ranged from (0.34, 0.34) to (0.29, 0.32), which corresponded to the pump power densities from 1.75 W/cm^2 to 16.13 W/cm^2. The color coordinates shifted toward the blue region due to the fact that the intensity of the blue emission increased faster than the green and red ones. Even more interesting was the fact that the

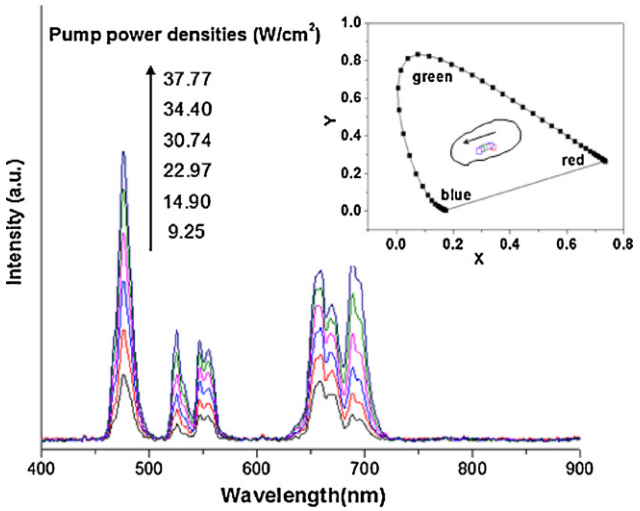

Fig. 9. Upconversion emission spectra and corresponding CIE chromaticity diagrams (see the inset) of 1931 together with the calculated color coordinates under different pump power of α-TeO_2:Tm^{3+}/Er^{3+}/Yb^{3+} (0.5/0.25/10 mol%) nanoparticles.

calculated color coordinates changed only slightly when the incident laser densities were varied between 1.75 and 16.13 W/cm^2.

4. Conclusions

The upconversion white luminescence of TeO_2:Tm^{3+}/Er^{3+}/Yb^{3+} nanoparticles were investigated in the present work. The as-prepared TeO_2:Tm^{3+}/Er^{3+}/Yb^{3+} nanoparticles showed the blue (476 nm), green (525 nm, 545 nm) and red (667 nm) emissions under 980 nm excitation. The combination of blue (from Tm^{3+}), green (from Er^{3+}) and red (from Er^{3+}) emissions resulted in the white luminescence, which was intense and visible to the naked eyes. The calculated CIE color coordinates of the TeO_2:Tm^{3+}/Er^{3+}/Yb^{3+} (0.5/0.25/10 mol%) nanoparticles fell well within the white region and changed little with the incident pump power. Thus, TeO_2 nanoparticles are potential host materials for upconversion white luminescent and TeO_2:Tm^{3+}/Er^{3+}/Yb^{3+} nanoparticles may be promising for the development of devices such as white light lasers and LEDs.

Acknowledgments

This work was supported by National Natural Science Foundation of China (21075053). We thank Professor Qinyuan Zhang at South China University of Technology for his assistance in luminescence decay curves detection.

References

[1] J. Lee, J. Choi, X.M. Zhang, J. Lee, K. Park, J. Kim, Mater. Lett. 64 (2010) 768–770.
[2] B.L. Wang, L.Z. Sun, H.D. Ju, S.L. Zhao, D.G. Deng, H.P. Wang, S.Q. Xu, Mater. Lett. 63 (2009) 1329–1331.
[3] J.W. Wang, P.A. Tanner, J. Am. Chem. Soc. 132 (2010) 947–949.
[4] T. Pang, W.H. Cao, M.M. Xing, X.X. Luo, X.F. Yang, Opt. Mater. 33 (2011) 485–489.
[5] M. Nyman, M.A. Rodriguez, L.E. Shea-Rohwer, J.E. Martin, P.P. Provencio, J. Am. Chem. Soc. 131 (2009) 11652–11653.
[6] D.L. Yang, H. Gong, E.Y.B. Pun, X. Zhao, H. Lin, Opt. Express 18 (2010) 18997–19008.
[7] A. Santana-Alonso, J. Mendez-Ramos, A.C. Yanes, J. del-Castillo, V.D. Rodriguez, Mater. Chem. Phys. 124 (2010) 699–703.
[8] E. Downing, L. Hesselink, J. Ralston, R. Macfarlane, Science 273 (1996) 1185–1189.
[9] H. Desirena, E. De la Rosa, P. Salas, O. Meza, J. Phys. D: Appl. Phys. 44 (2011) 455308/1–455308/4.
[10] H.T. Amorim, M.V.D. Vermelho, A.S. Gouveia-Neto, F.C. Cassanjes, S.J.L. Ribeiro, Y. Messaddeq, J. Solid State Chem. 171 (2003) 278–281.
[11] N.K. Giri, K. Mishra, S.B. Rai, J. Fluoresc. 21 (2011) 1951–1958.
[12] X. Hou, S. Zhou, T. Jia, H. Lin, H. Teng, J. Alloys Compd. 509 (2011) 2793–2796.
[13] Y. Li, J. Zhang, Y. Luo, X. Zhang, Z. Hao, X. Wang, J. Alloys Compd. 21 (2011) 2895–2900.
[14] V. Mahalingam, R. Naccache, F. Vetrone, J.A. Capobianco, Opt. Express 20 (2012) 111–119.
[15] X.L. Pang, C.H. Jia, G.Q. Li, W.F. Zhang, Opt. Mater. 34 (2011) 234–238.
[16] T. Passuello, F. Piccinelli, M. Pedroni, M. Bettinelli, F. Mangiarini, R. Naccache, F. Vetrone, J.A. Capobianco, A. Speghini, Opt. Mater. 33 (2011) 643–646.
[17] J.J. Li, L.W. Yang, Y.Y. Zhang, J.X. Zhong, C.Q. Sun, P.K. Chu, Opt. Mater. 33 (2011) 882–887.
[18] J.E.C. da Silva, G.F. de Sa, P.A. Santa-Cruz, J. Alloys Compd. 344 (2002) 260–263.
[19] A.S. Gouveia-Neto, L.A. Bueno, R.F. do Nascimento, E.A. da Silva, E.B. da Costa, V.B. do Nascimento, Appl. Phys. Lett. 91 (2007) 09114/1–09114/3.
[20] C. Zhao, Q.Y. Zhang, G.F. Yang, Z.H. Jiang, J. Fluoresc. 18 (2008) 87–91.
[21] Y.X. Zhou, J. Wang, S.X. Dai, T.F. Xu, Q.H. Nie, S.L. Huang, J. Lumin. 129 (2009) 1–5.
[22] I. Jlassi, H. Elhouichet, M. Ferid, C. Barthou, J. Lumin. 130 (2010) 2394–2401.
[23] J. Jakutis, L. Gomes, C.T. Amancio, L.R.P. Kassab, J.R. Martinelli, N.U. Wetter, Opt. Mater. 33 (2010) 107–111.
[24] R. Balda, J. Fernandez, J.M. Fernandez-Navarro, Opt. Express 17 (2009) 8781–8788.
[25] A.E. Ersundu, G. Karaduman, M. Celikbilek, N. Solak, S. Aydin, J. Alloys Compd. 508 (2010) 266–272.
[26] S.M. Salem, J. Alloys Compd. 503 (2010) 242–247.
[27] L.M.S. El-Deen, M.S. Al Salhi, M.M. Elkholy, J. Alloys Compd. 465 (2008) 333–339.
[28] N. Berkaine, E. Orhan, O. Masson, P. Thomas, J. Junquera, Phys. Rev. B 83 (2011) 245205/1–245205/10.
[29] P. Mosner, K. Vosejpkova, L. Koudelka, Thermochim. Acta 522 (2011) 155–160.
[30] R. Balda, M. Al-Saleh, A. Miguel, J.M. Fdez-Navarro, J. Fernandez, Opt. Mater. 34 (2011) 481–486.
[31] G. Bilir, N. Mustafaoglu, G. Ozen, B. DiBartolo, Spectrochim. Acta A 83 (2011) 314–321.
[32] B.Y. Qin, Y. Bai, Y.H. Zhou, J. Liu, X.Y. Xie, W.J. Zheng, Mater. Lett. 63 (2009) 1949–1951.
[33] H. Hu, Y. Bai, M.W. Huang, B.Y. Qin, J. Liu, W.J. Zheng, Opt. Mater. 34 (2011) 274–277.
[34] Y.Q. Sheng, J. Liu, L.L. Xu, D. Zhai, Z.G. Zhang, W.W. Cao, Solid State Commun. 150 (2010) 1048–1051.
[35] J. Yang, C.M. Zhang, C. Peng, C.X. Li, L.L. Wang, R.T. Chai, J. Lin, Chem. Eur. J. 15 (2009) 4649–4655.
[36] L. Sun, A.H. Li, F.Y. Guo, Q. Lü, Y.H. Xu, L.C. Zhao, Appl. Phys. Lett. 91 (2007) 071914/1–071914/3.
[37] H.X. Zhang, C.H. Kam, Y. Zhou, X.Q. Han, S. Buddhudu, Q. Xiang, Y.L. Lam, Y.C. Chan, Appl. Phys. Lett. 77 (2000) 609–611.
[38] Y.P. Li, J.H. Zhang, Y.S. Luo, X. Zhang, Z.D. Hao, X.J. Wang, J. Mater. Chem. 21 (2011) 2895–2900.